A Simple Model Relating Gauge Factor to Filler Loading in Nanocomposite Strain Sensors

James Garcia[1], Domhnall O'Suilleabhain[1], Harneet Kaur[1] and Jonathan N. Coleman[1]*

[1]*School of Physics, CRANN & AMBER Research Centres, Trinity College Dublin, Dublin 2, Ireland*

*colemaj@tcd.ie (Jonathan N. Coleman); Tel: +353 (0) 1 8963859.

ABSTRACT: Conductive nanocomposites are often piezoresistive, displaying significant changes in resistance on deformation, making them ideal for use as strain and pressure sensors. Such composites typically consist of ductile polymers filled with conductive nanomaterials, such as graphene nanosheets or carbon nanotubes, and can display sensitivities, or gauge factors, which are much higher than those of traditional metal strain gauges. However, their development has been hampered by the absence of physical models which could be used to fit data, or to optimise sensor performance. Here we develop a simple model which results in equations for nano-composite gauge factor as a function of both filler volume fraction and composite conductivity. These equations can be used to fit experimental data, outputting figures of merit, or predict experimental data once certain physical parameters are known. We have found these equations to match experimental data, both measured here and extracted from the literature, extremely well. Importantly, the model shows the response of composite strain sensors to be more complex than previously thought and shows factors other than the effect of strain on the interparticle resistance to be performance-limiting.

KEYWORDS: piezoresistor; strain sensor; graphene; nanotube, tunnelling

INTRODUCTION

Incipient technological developments such as the internet of things, smart cities and personalised medicine will require everything from packaging to buildings to clothing to gather, process and exchange information. A critical part of this revolution will involve the proliferation of sensors and sensing technologies.[1, 2] Of the different sensor types, strain and pressure sensors are conceptually simple and have applications in a range of areas including biomedical sensing, sports performance monitoring and robotics.[3, 4] Such sensors are usually based on piezoresistive materials which display changes in electrical resistance as they are deformed.

While an effective strain sensor must display a number of appropriate characteristics (e.g. sufficient working range,[5] reasonable conductivity, lack of frequency or rate-dependence[6]), probably the most important property is the sensitivity or gauge factor, *G*. This figure of merit is defined via $\Delta R / R_0 = G\varepsilon$, where $\Delta R / R_0$ is the fractional resistance change in response to an applied strain, ε. Strictly speaking, this equation applies at low strains, where $\Delta R / R_0$ varies linearly with strain such that *G* has a well-defined value. By far the most common type of strain sensors are metal foil strain gauges which are cheap and effective and are widely used in industry. However they have some significant drawbacks, namely, relatively small gauge factors of $G \sim 2$.[7] Such a small value means a very limited sensitivity and has driven the research community to search for sensing platforms which display much higher sensitivities.

To resolve this issue, many researchers have turned to materials science and in particular, polymer-nanocomposites. Such composites are widely used due to their processability, flexibility and low cost. Extensive research has underlined the versatility of polymer-nanocomposites where materials can be tailored to display a range of desired properties such as excellent conductivity, mechanical reinforcement, electro-magnetic interference shielding, enhanced thermal stability and polymer self-healing.[8-12] Piezoresistive nanocomposites, have proved particularly promising in the area of strain sensing as they display impressive and tuneable sensitivities which far surpass current commercially available strain sensors.[5, 13] These nanocomposites contain conductive nanoparticles dispersed within an insulating matrix, typically a polymer. While nanocomposites utilising fillers such as Graphene[14-18] and CNTs[19-21] have been widely investigated, piezoresistive behaviour has been observed with a host of other nanofillers such as conductive polymers,[22] carbon black[23, 24], silver nanowires[25], carbon fibres[26] and semiconducting materials.[27, 28]

The electrical properties of conductive composites are understood in great detail, with much experimental and theoretical work (e.g. via percolation theory) having been carried out in recent years.[17, 29] As a result, one might imagine that the piezoresistive properties of such composites would be well understood. However, this is not the case. Although it is generally believed that the effect of strain on interparticle tunnelling is responsible for the piezoresistive effect in nanocomposites,[19, 30-32] good analytical models are not available. A number of numerical studies on the piezoresistive response in nanocomposites exist,[19, 25, 31] with the recent work of Liu et al. allowing a visualisation of the conductive network evolution under tensile strain.[33, 34] However, these studies are filler specific and cannot be universally applied. What is needed are straightforward models which yield simple equations, which describe how G varies with ϕ or indeed composite conductivity. Such models would allow the fitting of experimental data and give an insight into the nanocomposite properties which determine the gauge factor. Ultimately, this would allow for the development nanocomposites with enhanced values of *G*.

In this study, we use percolation theory to develop a simple model relating the gauge factor (G) of nano-composite piezoresistive materials to both the filer volume fraction (ϕ) and the zero-strain conductivity, σ_0. This model's accuracy is tested against a number of composites with different conductive fillers and is supported by a detailed study of how percolation parameters vary with applied strain.

RESULTS AND DISCUSSION

Electrical Percolation

By now, much is known about the conductivity in nanocomposites. Most importantly, they show large increases in conductivity as filler loading is increased. As ϕ is increased above a critical value, the percolation threshold (ϕ_c), the first continuous conductive paths spanning the length of the sample are formed, allowing current to flow. Above the percolation threshold (i.e. $\phi > \phi_c$) the conductivity is usually described using classical percolation theory,[35-37] which in its simplest form yields:

$$\sigma = \sigma_c(\phi - \phi_c)^t \qquad (1)$$

where σ_c is a constant and *t* is the percolation exponent.

Many papers have been devoted to understanding the nature of ϕ_c, σ_c and t. In a random network of non-spherical particles such as nanotubes or graphene sheets, the percolation threshold is expected to be roughly equal to the ratio of small to large particle dimensions (e.g. nanosheet thickness over length).[38, 39] However, if the particle orientation distribution becomes less random, for example, if the particles become aligned, ϕ_c can increase significantly.[40-42] In addition, σ_c has been linked to the junction resistance between particles,[38] which may be controlled by tunnelling[15] or hopping,[43] and so is sensitive to inter-particle separation.

The percolation exponent, t, was originally expected to take universal values of t_{un}=1.3 or 2 depending on whether the system in question was 2- or 3-dimensional.[44] However, multiple experimental observations of t>2 has led to theoretical work that shows that t can indeed be larger than the universal value, t_{un}. The current consensus is that, where there is a distribution of inter-particle resistances, t-t_{un} is controlled by the width of the inter-particle junction resistance distribution.[44-46] In polymer-based composites, we would expect disordered regions of polymer to separate the conductive particles leading to a distribution of interparticle separations and so resistances, resulting in values of t>2.[29]

Model Development

Any model which describes the performance of nanocomposite strain sensors must be consistent with experimental data which means it must display certain general features. For example, almost all reports in the literature suggest that the gauge factor is highly dependent on the loading of conductive filler, with the gauge factor decreasing rapidly as the filler volume fraction is increased above the percolation threshold.[15, 19] This means that increasing gauge factor is associated with decreasing conductivity as reported in a number of papers.[15, 19, 47-53] A review of the literature identified a number of papers which reported both conductivity (at zero-strain) and gauge factor for various composites each measured at a range of filler loadings.[15, 19, 50] As shown in figure 1, these data sets are suggest a roughly power-law relationship between gauge factor (G) and zero-strain conductivity (σ_0). Any successful model describing nanocomposite strain sensors must describe the dependence of G on both ϕ and σ_0 in a way that is consistent with these findings and be applicable across the broad range of strain sensing materials.

When a material is strained, the resistance changes for two reasons. Firstly, there is a relatively small change due to the effect of strain on the sample dimensions – this is dominant in metallic

strain gauges. Secondly, the resistance can change due to variations in the material conductivity with strain.[7] The second effect can be positive[15, 16] or negative[28] and can be very large in some systems,[15] including nanocomposites.

These effects can be quantified in a simple model which shows that [see ref [3, 15] and SI]

$$G \approx 2 - \frac{1}{\sigma_0}\left(\frac{d\sigma}{d\varepsilon}\right)_0 \qquad (2)$$

Where the subscript zero means the quantity must be taken in the limit of low-strain such that σ_0 denotes the zero-strain conductivity. This low-strain condition comes from approximations in the derivation that are valid only at low-strain (see SI).

This equation can be applied to percolative systems by differentiating equation 1 with respect to strain, assuming ϕ_c, σ_c and t all depend on strain. Performing this differentiation (see SI) yields:

$$\frac{d\sigma}{d\varepsilon} = \sigma_c(\phi-\phi_c)^t\left[\frac{1}{\sigma_c}\frac{d\sigma_c}{d\varepsilon} + \frac{dt}{d\varepsilon}\ln(\phi-\phi_c) - t\frac{d\phi_c}{d\varepsilon}(\phi-\phi_c)^{-1}\right] \qquad (3)$$

This equation can be combined with equation 2 by taking all parameters in their low-strain limits. In that limit, $\sigma \simeq \sigma_0$ and by extension $\sigma_c \simeq \sigma_{c,0}$, $\phi_c \approx \phi_{c,0}$ and $t \simeq t_0$. This gives

$$G \approx 2 - \frac{1}{\sigma_{c,0}}\left(\frac{d\sigma_c}{d\varepsilon}\right)_0 - \left(\frac{dt}{d\varepsilon}\right)_0 \ln(\phi-\phi_{c,0}) + \left(\frac{d\phi_c}{d\varepsilon}\right)_0 \frac{t_0}{\phi-\phi_{c,0}} \qquad (4a)$$

This equation links the nanocomposite gauge factor to both the zero-strain percolation parameters $\sigma_{c,0}$, $\phi_{c,0}$ and t_0 as well as their derivatives, measured at low strain, $\left(d\sigma_c/d\varepsilon\right)_0$, $\left(d\phi_c/d\varepsilon\right)_0$ and $\left(dt/d\varepsilon\right)_0$. An important feature of this equation is that *G* scales with $(\phi-\phi_{c,0})^{-1}$ which would explain the experimental observation that *G* increases sharply as the percolation threshold is approached from above.

We note that, because of the way equation 1 is generally used to fit conductivity versus ϕ data (plotting $\ln\sigma_0$ versus $\ln(\phi-\phi_{c,0})$ to obtain $\ln\sigma_c$ and t_0 as fit parameters), some researchers will prefer to write equation 4a as:

$$G \approx \left[2 - \left(\frac{d\ln\sigma_c}{d\varepsilon}\right)_0\right] + \left[\left(\frac{dt}{d\varepsilon}\right)_0 \ln(\phi-\phi_{c,0})^{-1}\right] + \left[\left(\frac{d\phi_c}{d\varepsilon}\right)_0 \frac{t_0}{\phi-\phi_{c,0}}\right] \qquad (4b)$$

We can use equation 4b to generate an equation for G in terms of the zero-strain conductivity, σ_0, by noting that at zero-strain, equation 1 shows that $\sigma_0 = \sigma_{c,0}(\phi - \phi_{c,0})^{t_0}$, leading to:

$$G \approx \left[2 - \left(\frac{d\ln\sigma_c}{d\varepsilon}\right)_0\right] + \left[\frac{1}{t_0}\left(\frac{dt}{d\varepsilon}\right)_0 \ln\left(\frac{\sigma_{c,0}}{\sigma_0}\right)\right] + \left[t_0\left(\frac{d\phi_c}{d\varepsilon}\right)_0\left(\frac{\sigma_{c,0}}{\sigma_0}\right)^{1/t_0}\right] \quad (4c)$$

We have written these equations in what might seem an unusual fashion for two reasons: to clearly differentiate the three square-bracketed terms and to facilitate a clear discussion of the sign of each term (see below). As these equations make clear, there are a number of factors, embodied by the three square-bracketed terms, which contribute to the gauge factor. We will consider these factors below.

The factors contributing to the gauge factor

One advantage of this approach is that our understanding of electrical percolation can be used to understand nanocomposite piezoresistivity. The factors influencing the percolation parameters, $\phi_{c,0}$, $\sigma_{c,0}$ and t_0 have been outlined above. Clearly, such factors will influence *G* via equations 4b and 4c. For example, the dispersion state of the filler will affect $\phi_{c,0}$, with filler alignment[42] leading to higher $\phi_{c,0}$, compared to randomly oriented[54] systems. According to figure 4b, reducing $\phi_{c,0}$ should lead to smaller gauge factor for a given ϕ. Polymer morphology will also have an impact. If the polymer tends to crystalise on the nano-filler surface, this will increase the inter-particle resistance, thus[38] decreasing $\sigma_{c,0}$. Equation 4c shows that this will reduce *G* at a given compsoite conductivity. It is worth considering how the other parameters in equations 4b-c impact *G*.

The first term in equations 4 b-c is dominated by the rate of change of $\ln\sigma_c$ with ε (at low strain), $(d\ln\sigma_c/d\varepsilon)_0$. To understand this term, we note that in most (but not all)[28] polymer-based nanocomposites, where the fillers are highly conductive, we expect σ_c to be limited by the junction resistance (R_J) between filler-particles such that $\sigma_c \propto 1/R_J$.[38] Whether the inter-sheet transport is via hopping or tunnelling,[15, 43] we expect $R_J \propto e^{kd}$, where *d* is the inter-particle separation (at a given strain) and *k* is a (positive) constant. Assuming that, on application of tensile strain, the inter-particle separation scales with sample length, then $\varepsilon = (d - d_0)/d_0$, where d_0 is the zero-strain inter-particle separation. Combining these ideas

gives: $d\ln\sigma_c / d\varepsilon = -kd_0$, showing that $(d\ln\sigma_c / d\varepsilon)_0$ should be negative (unless the inter-particle charge transfer is not rate limiting[28]). This negative sign is expected and is in line with many studies showing composites to become more resistive on tensile deformation.[15, 16, 19, 25, 31, 55] This negative sign is significant as it means the first square bracketed term in equations 4 b and c must be positive.

Thus, the first term in equations 4 b-c is predominantly associated with inter-particle transport and describes the mechanism traditionally used to describe the piezoresistive response in nanocomposites.[19, 30-32] However, the existence of two other terms in equations 4 b-c shows that this is not the only contribution to G.

The second term in equations 4 b-c is controlled by the strain dependence of the percolation exponent, $(dt / d\varepsilon)_0$. A number of papers have shown that the value of *t* is controlled by the width of the distribution of inter-particle junction resistances.[44-46] Then, strain would most likely increase each individual junction separation according to $d = d_0(\varepsilon + 1)$, thus broadening the distribution and increasing *t*. Alternatively, strain should align the particles somewhat, making the network more 2D and less 3D and so reducing *t*.[32] Thus, we expect the second term to be controlled by a combination of junction and network effects, each driving $(dt / d\varepsilon)_0$ in different directions. We note that theoretical calculations have suggested that $\left(d\ln\sigma_c / d\varepsilon\right)_0 \propto \left(dt / d\varepsilon\right)_0$ such that both parameters have the same sign.[46] If this were true it would mean that $\left(dt / d\varepsilon\right)_0$ is generally negative. This is important as it means that the second term in equations 4b-c should be negative. This has important implications as we will discuss below.

The third term in equations 4 b-c is controlled by the strain dependence of the percolation threshold, $\left(d\phi_c / d\varepsilon\right)_0$. It is likely that the application of strain alters the structure of the network, for example by inducing particle alignment, in a way that modifies the percolation threshold. To see this, consider a composite exactly at the percolation threshold. Then, all current flows through a single conducting path with a well-defined bottleneck (where all current flowing through a single inter-particle junction). While application of tensile strain would be very unlikely to create new paths, it is likely that the strain-induced change to the network structure will break the bottleneck. This will destroy the single conducting path and shift the percolation threshold (at that strain) to higher filler volume fraction. Thus, we always

expect $\left(df_c/d\varepsilon\right)_0$ to be positive. This is important as it means the third term in equations 4 b and c must always be positive. This is consistent with previous studies which investigated the effect of carbon nanotube (CNT) alignment on film conductivity (with alignment acting as a proxy for tensile strain). Such studies show that as alignment increases the percolation threshold similarly increases.[40, 41]

Thus, in addition to the effect of strain on inter-particle transport, which is usually considered as the mechanism controlling *G*, there are other factors related to both properties of the junctions and the network which contribute to *G*. Later in this paper, we will consider the relative magnitude of these effects. However, first it is necessary to demonstrate that the equations above can actually describe experimental data.

Using this model to fit experimental data

While equations 4b and 4c provide a theoretical description of the dependence of *G* on ϕ and σ_0 respectively, neither equation can be used in their current form for fitting experimental data, simply because they both contain too many fit parameters. However, they can both be simplified by considering the contributions to the second and third terms of equations 4 b-c. Since $\ln(f - f_c)$ is a slow varying function compared to $(f - f_c)^{-1}$ as $\phi \to \phi_{c,0}$, it is likely that the second term of equations 4 b-c is relatively slowly varying compared to the third. This allows us to consider the second term constant for fitting purposes, assuming that $(dt/d\varepsilon)_0$ is not far larger than $t_0(df_c/d\varepsilon)_0$ (this will be justified further below). Applying this approximation to both equations 4b and 4c and grouping terms allows us to write equations for G in the form:

$$G \approx G_{0,\phi} + \frac{G_1}{\phi - \phi_{c,0}} \qquad (5a)$$

$$G \approx G_{0,\sigma} + (\sigma_1/\sigma_0)^{1/t_0} \qquad (5b)$$

Where $\phi_{c,0}$, $G_{0,\phi}$, G_1, $G_{0,\sigma}$ and σ_1 are (near) constants. To maximise *G*, requires all of these constants except $\phi_{c,0}$ to be large and positive. We note that this model implies that *G* has near power-law relationship with σ_0, which is consistent with observations in figure 1.

To test our models, we have prepared graphene-polymer composites using two siloxane-based polymer matrices (see Schematic 1 and methods). One matrix was the commercially available

sylgard polymer which was chemically cross-linked by curing (Fig 2A). The other was a homemade material made by mixing silicone oil with boric acid to yield a soft polymer similar to silly putty which, when mixed with graphene, results in a composite known as G-putty (Fig 2B).[15, 56] To achieve this, graphene nanosheets (Fig 2C) were prepared via liquid phase exfoliation with a typical lateral size of ~511nm (Fig 2D) and an average layer thickness, <N> = 12 layers (Fig 2E) was determined from uv-vis measurements using previously published metrics.[57] Raman spectra for graphene nanosheets as well as G-putty and graphene-sylgard composites consist of the D, G and 2D bands as expected. The low intensity of the D band indicates the graphene to be defect free while the shape of the 2D band is consistent with few layer graphene.[57] In each case, we prepared composites for a range of graphene volume fractions, before measuring the zero-strain conductivity (σ_0) and the gauge factor (G) via resistance-strain measurements, each at a range of graphene volume fractions (see SI for electro-mechanical characterisation).

Shown in figure 3A are values of (σ_0) plotted versus ϕ for both composite types. The solid lines represent fits to equation 1 (see table 1 for fit parameters). In addition, figure 3B shows a linearized version of figure 2A, illustrating the excellent agreement between data and model. In both cases, the fit parameters are consistent with previous results. Here we obtained $\phi_{c,0}$ = 3.4vol% and $\phi_{c,0}$ = 5.5vol% for G-putty and graphene sylgard composites. While these percolation thresholds are relatively high, a review of graphene-polymer composites by Marsden et al.[17] demonstrates that a broad range of percolation threshold values exists, 0.004 – 5 vol%, for nanocomposites with graphene and other carbon based fillers. Additionally, Wang et al.[53] report a similar graphene-siloxane based sensor with $\phi_{c,0}$ = 8.1vol%.

Our values of σ_c were 3.3×10^3 S/m and 4.6×10^7 S/m for G-putty and graphene-sylgard composites. Literature values for σ_c vary over many orders of magnitude. For example epoxy-graphene composites have been reported with values as low as $\sigma_c \sim 10^{-6}$ S/m,[58] whereas polystyrene- graphene composites have been shown to give $\sigma_c \sim 10^5$ S/m.[54] The values reported here lie at the upper end of the literature.

The percolation exponents were 5.4 and 5.1 for G-putty and graphene sylgard composites. We note that the percolation exponents are both somewhat higher than the universal value of t_{un}=2 in 3D. This is very common[29] for polymer-based nanocomposites with higher values of t indicating the presence of a broad distribution of inter-nanosheet junction resistances.[44-46]

As is almost[28] always observed, the nanocomposite resistance increased with strain (figure 3 C-D), a fact that is usually attributed to the effect of strain on inter-particle junctions.[19, 25, 31] In all cases, the fractional resistance change scaled linearly with strain at low strain with some non-linearity appearing at strains above ~0.75%. In these curves the low-strain slope is equal to the gauge factor which has been extracted for a range of volume fractions for each composite type.

The resultant gauge factors have been plotted versus ϕ in figure 3E for both composite types. We have fit both data sets using equation 5a, finding very good matches (see table 1 for fit parameters). In both cases, the data (and fit) diverge as $\phi \to \phi_{c,0}$ from above, in line with the prediction of equation 5a. In order to best assess the agreement between data and model, we plot the data in a manner which, according to the model, should yield a straight line (figure 3F). This does indeed yield a straight line, confirming that the model describes the data very well and that the approach of treating the ln term in equations 4 b-c is a valid one. In addition, these fits introduce a somewhat unexpected fact, that the $G_{0,\phi}$ parameter (represented by the intercept in figure 3F can be negative. This will be discussed in more detail below.

As shown in figure 3G, we have also plotted the gauge factor versus the zero-strain composite conductivity (reproduced from figure 1). We have fitted both data sets to equation 5b, again getting good agreement (see Table 1 for fit parameters). In addition, we demonstrate the fidelity of the model to the data by plotting the data in a linearized fashion in figure 3H, again finding very good agreement.

Fit parameters

As described above, standard strain sensor measurements lead to three distinct data sets (σ_0 vs. ϕ, G vs. ϕ and G vs. σ_0) that can be fit using equations 1, 5a and 5b yielding nine fit parameters as listed in table 1. It is clear from table 1 that there is some degree of redundancy in these fit parameters. For example, the percolation threshold ($\phi_{c,0}$) can be extracted from fitting both σ_0 vs. ϕ and G vs. ϕ data while the percolation exponent (t_0) can be extracted from fitting σ_0 vs. ϕ and G vs. σ_0 data sets. In addition, inspection of equations 4b and 4c, in combination with equation 1, shows that the parameters $G_{0,\phi}$ and $G_{0,\sigma}$ are actually identical. Thus, under normal circumstances, it would not be necessary to fit all three data sets, with most researchers probably opting to fit only σ_0 vs. ϕ and G vs. ϕ.

While the percolation fit parameters ($\sigma_{c,0}$, $\phi_{c,0}$ and t_0) are well known, obviously the parameters where $G_{0,\phi}$, G_1, $G_{0,\sigma}$ and σ_1 will be new to readers. It is important to assess the range of values these parameters can take in composites. To achieve this, we have used equations 5 a-b to fit the published data sets shown in figure 1 (see SI). This analysis shows that $G_{0,\phi}$ and $G_{0,\sigma}$ can both display values between -200 and 80. In addition, we find the minimum ranges of G_1 and σ_1 to be $10^{-2} < G_1 < 10^{2}$, and $10^{-4} < \sigma_1 < 10^{13}$ (see SI).

Rate of change of percolation parameters with strain

The analysis above shows equations 5 a-b to accurately represent experimental data. However, it would be ultimately more useful to determine how accurately equations 4b-c match experimental data, as it is these equations which contain the physics describing the piezoresistive process. As we already have data for $\sigma_{c,0}$, $\phi_{c,0}$ and t_0, testing these equations requires knowledge of $\left(d\ln\sigma_c / d\varepsilon\right)_0$, $\left(d\phi_c / d\varepsilon\right)_0$ and $\left(dt / d\varepsilon\right)_0$. To obtain these parameters, we first take the resistance versus strain measurements (at 0.2% strain increments) recorded for various volume fractions (e.g figure 3 C-D) and convert them to resistance versus volume fraction data sets, each at various strains (limiting ourselves to strains from 0 to 2%). For each strain, the set of resistances were converted to conductivity assuming constant sample volume:

$$\sigma = R\frac{L_0}{A_0}(\varepsilon+1)^2 \qquad (6)$$

where L_0 and A_0 are the zero-strain sample length and cross-sectional area. This procedure yields a set of conductivity versus volume fraction data sets, each at a different strain. Examples of such curves, associated with strains of 0% and 2% are shown in figures 4 A-B. These curves clearly show slight reductions in conductivity with strain at all volume fractions. These curves were then fit to the percolation scaling law (equation 1) yielding values of $\ln\sigma_c$, ϕ_c and t as a function of strain for each composite as plotted in figure 4 C-H.

As shown in figures 4 C-D, both composites show reductions in $\ln\sigma_c$ with increasing strain, although for the graphene-sylgard composites the change is small compared to the error bars. Notwithstanding the error, the low-strain values of $\left(d\ln\sigma_c / d\varepsilon\right)_0$ are -4.4 and -120 for graphene-sylgard and G-putty composites respectively. This can be compared with values of

$d \ln \sigma_c / d\varepsilon \approx$-30 which can be extracted from ref[32]. As described above, we expect these slopes to be negative.

The values of $d \ln \sigma_c / d\varepsilon = -kd_0$ are different by a factor of 27 between the graphene-sylgard and G-putty composites. If a non-trivial amount of inter-particle charge transport is to occur, the value of d_0 must lie in a relatively narrow range (d_0 can never be less than the van der Waals distance while values greater than a few nm will result in negligible tunnelling current). This means that much of this large difference is probably associated with variations in k between composites. As k is presumably controlled by the details of the inter-particle potential barrier, this shows that the nature of the junction can have a significant impact on the gauge factor.

Both composites also show reductions in t with increasing strain (figures 4E-F). However, as before, the graphene-sylgard composites show a small change compared to the size of the error bars. The low-strain values of $\left(dt / d\varepsilon\right)_0$ are -4.2 and -33 for graphene-sylgard and G-putty composites respectively. Both of these results show a reduction in t with strain, consistent with the only other published work we could find on this topic.[32] Zhang et al investigated electromechanical properties of MWCNT- polyurethane composites, finding $\left(dt / d\varepsilon\right)_0$=-8.[32] We note that this value has the same sign as $\left(d \ln \sigma_c / d\varepsilon\right)_0$, as indicated above.

As shown in both figure 4 G-H, both composites show a clear increase of percolation threshold with strain, leading to low-strain slopes, $\left(d\phi_c / d\varepsilon\right)_0$, of 0.07 and 0.5 for graphene-sylgard and G-putty composites respectively. These results agree with previous studies which showed increases in percolation threshold both with strain[32] and under alignment.[59] For example, Zhang et al. measured $\left(d\phi_c / d\varepsilon\right)_0$=0.004 for polyurethane-nanotube composites.[32] Such positive slopes are to be expected as described above.

Using these derivatives to model the gauge factor

Once values for all of the quantities in equations 4b and 4c are known, these equations can be used to plot numerical graphs of G vs. ϕ and G vs. σ_0. Comparison with experimental data would provide evidence as to the accuracy of equations 4 b and c. Substituting values of $\sigma_{c,0}$, $\phi_{c,0}$ and t_0 from table 1 (choosing the values appropriate to each graph and each material), as well as values for $\left(d \ln \sigma_c / d\varepsilon\right)_0$, $\left(d\phi_c / d\varepsilon\right)_0$ and $\left(dt / d\varepsilon\right)_0$ (table 2) for both graphene-

sylgard and G-putty composites into equations 4b and c yields plots of G vs. ϕ and G vs. σ_0 as shown in figure 4 (black lines). These curves match the experimental data extremely well, illustrating the validity of our approach.

This agreement between model-prediction and data allows us to assess the magnitude of the contributions of each term in equations 4b-c. We use the same parameters as before to plot each term individually on each panel in figure 5. The first thing to note is that the second term (blue line) depends only weakly on ϕ and σ_0 justifying our assertion that the ln terms could be treated as constant. In addition, the first (green line) and third (red line) terms are positive while the second term (blue line) is negative as described above. In addition, the first and second terms are similar in magnitude which means that they somewhat cancel each other out. Depending on the degree of cancelation, this can result in relative small or negative values of $G_{0,\phi}$ and $G_{0,\sigma}$, limiting the positive contribution of the first two terms to the gauge factor. Essentially, this means that the third term can be particularly important, especially for volume fractions approaching the percolation threshold.

The fact that equations 4b and 4c describe experimental data so well means we should revisit the assertion, made earlier, that these equations should not be used to fit data (we suggested using equations 5a-b). Both equation 4b and 4c have 5 fit parameters, which is too many to allow reliable fitting of standard data sets. However, it is worth considering if equations 4b and 4c can be used for fitting data in order to obtain values for $d\sigma_c/d\varepsilon$, $d\phi_c/d\varepsilon$ and $dt/d\varepsilon$ if the percolation fit parameters ($\sigma_{c,0}$, $\phi_{c,0}$, t_0) were used as fixed values. We attempted to achieve this for the graphene-sylgard and G-putty data sets as shown in the SI. We achieved mixed results, obtaining some reasonable values of $d\sigma_c/d\varepsilon$, $d\phi_c/d\varepsilon$ and $dt/d\varepsilon$ and some results which were far from the expected values or which had large errors. We believe the main problem here is associated with the limited number of data points per data set (6 in this case). Although such data sets are standard or even extensive compared to the literature, they are clearly not enough to reliably extract the derivatives. However, this might be addressed in future, simply by fabricating larger sample sets with more filler volume fractions, leading to more data points per data set.

Factors effecting gauge factor

Now that it is reasonably clear that equations 4b and 4c can quantitatively describe experimental data, it is worth considering what we require of each parameter in order to maximise G. For simplicity, we will focus on equation 4b.

Ideally, we would want the sum of the first two terms to be large and positive. Given its expected negative sign, this means we want $|\left(d\ln\sigma_c/d\varepsilon\right)_0|$ to be as large as possible to maximise the first term. In addition, because we expect $\left(dt/d\varepsilon\right)_0$ and so the entire second term to be negative, we need $|\left(dt/d\varepsilon\right)_0|$ to be small while we would like t_0 to be large. However, if, as described above $\left(d\ln\sigma_c/d\varepsilon\right)_0 \propto \left(dt/d\varepsilon\right)_0$, it is clearly not possible to achieve these conditions simultaneously. If it were possible to engineer the properties of the composite, the most pragmatic strategy might be to maximise $|\left(d\ln\sigma_c/d\varepsilon\right)_0|$ and t_0 in the hope that $|\left(dt/d\varepsilon\right)_0|$ is not too large to negatively affect *G*. Maximising $|\left(d\ln\sigma_c/d\varepsilon\right)_0|$ means maximising the product kd_0 mentioned above. Clearly, to do this requires an understanding of the inter-particle transport mechanism and so *k*. However, if for example, the relevant mechanism is Simmon's tunnelling as assumed in refs [19, 30], then maximisation of *k* requires maximisation of the height of the inter-particle tunnelling barrier. This might be achievable by coating the conducting particles with a wide-bandgap insulator.

The third term in equation 4b is less ambiguous. This term will always be positive and will be maximised for large values of t_0 and $\left(d\phi_c/d\varepsilon\right)_0$. As mentioned above t_0 is associated with the width of the distribution of inter-particle junction resistances, a parameter that might somehow be engineered. The nature of $\left(d\phi_c/d\varepsilon\right)_0$ is less clear. However, we note that if t_0 is known (for example by fitting conductivity data), $\left(d\phi_c/d\varepsilon\right)_0$ can be obtained from G_1 (obtained by fitting *G* vs. ϕ data to equation 5a). To shed more light on what values of $\left(d\phi_c/d\varepsilon\right)_0$ are possible, we estimated $\left(d\phi_c/d\varepsilon\right)_0$ by fitting the literature data shown in figure 1 (see SI) to obtain G_1. These values were combined with the t_0 values from figure S9B (here we took the average of both t_0 values for each material) to obtain $\left(d\phi_c/d\varepsilon\right)_0$. To illustrate these values, we plot the resultant values of $\left(d\phi_c/d\varepsilon\right)_0$ versus t_0 as shown in figure 5. We find a well-defined relationship with larger values of t_0 leading to larger values of $\left(d\phi_c/d\varepsilon\right)_0$.

We can understand this relationship as follows. Large values of t_0 indicate a broad distribution of inter-particle junction resistances. Consider a composite with large t_0 very close to the

percolation threshold. Under these circumstances, only one complete current path exists which will have at least one bottleneck. The larger the value of t_0, the larger the probability is that the limiting inter-particle junction is one of high resistance. Because high-resistance junctions are likely to be associated with large inter-particle separation ($R_J \propto e^{kd}$), they are more likely to be broken under strain. Such breakage will destroy the current path, shifting the percolation threshold (at that strain) to higher filler volume fraction. We expect such circumstances to lead to high $\left(d\phi_c / d\varepsilon\right)_0$, illustrating the link between this parameter and t_0.

The discussion above illustrates the importance of t_0. This is probably the most important parameter of all due to its double influence on the third term in equation 4b as well as its role in reducing the magnitude of the (negative) second term. We believe that the maximisation of G would be significantly enhanced if it became possible to find ways to engineer composites to have high values of t_0.

CONCLUSION

In conclusion, we have used percolation theory to develop a model relating the nanocomposite gauge factor (sensitivity), to filler volume fraction in piezoresistive sensors. This model predicts the gauge factor to diverge as the filler volume fraction approaches the percolation threshold from above, a key feature observed experimentally for nanocomposite sensors. In addition, alongside the widely considered contribution from the interparticle resistance, the model shows the gauge factor to depend strongly on effects associated with the network of filler-particles.

The model is in good agreement with experimental data, both measured here and extracted from the literature. In addition, once the percolation fit parameters and their strain-derivatives were independently obtained from experimental data and inserted into the model, gauge factors could be predicted to a good degree of accuracy.

These results are important for two reasons. Firstly, our equations can be used to fit experimental data, yielding figures of merit for piezoresistive performance. This allows the comparison of strain sensors both with each other and with the literature. More importantly, this work shows the response of composite strain sensors to be more complex than previously thought and shows the effect of strain on the particle network to be at least as important as the effect of strain on the interparticle resistance.

METHODS

Graphene

A graphene dispersion was prepared by ultra-sonic tip sonication (Hielscher UP200S, 200 W 24 kHz) of graphite (Branwell, Graphite Grade RFL 99.5) in 1-methyl-2-pyrrolidone (NMP) (Sigma Aldrich, HPLC Grade) at a concentration of 100mg/ml for 72hrs at an amplitude of 60%. The resulting dispersion then undergoes mild centrifugation at 1500rpm for 90 mins to remove unexfoliated aggregates and large nanosheets. The supernatant is then vacuum filtered on a 0.1um nylon membrane, forming a thick disk of re-aggregated graphene nanosheets. This disk was then ground into a fine powder using a mortar & pestle before being added to separate solutions of Chloroform (10mg/ml) and IPA (1mg/ml). Graphene was then redispersed in each solvent by tip sonication for 90mins at 40% amplitude to form stock solutions.

G-Putty

G-putty is a viscoelastic siloxane-based graphene composite described in previous works.[15, 56]

Firstly, silicone oil is partially crosslinked using boric acid which results in the formation of a material similar to Silly putty®. 2ml of Silicone oil (VWR CAS NO: 63148-62-9, 350 cSt) was added to a 28ml glass vial. Boric Acid (Sigma Aldrich 99.999% trace metal basis CAS: 10043-35-3) was ground with a mortar and pestle until a fine powder was formed. This powder was then added to the silicone oil at a concentration of 0.4 g/ml and stirred by magnetic stirrer bars until the mixture was homogenous and opaque. The glass vials were then added 6 at a time to a specially prepared aluminium holder.

An oil bath was pre-heated to 175°C (IKA C-MAG HS 7 hotplate with the temperature controlled and monitored using an ETS-D5 thermometer), the aluminium holder was then submerged in the bath and the temperature was increased to 225°C. Silicone oil/Boric acid mixture was cured for ~2.5hrs (including heating time from 175°C to 225°C) under continuous magnetic stirring. The vials were then removed from the oil bath and allowed to cool. Once cooled the resulting material was a viscoelastic gum, which could be removed from the vials with a spatula.

0.5g of the viscoelastic gum was added to a beaker with the appropriate amount graphene-chloroform solution, depending on the required graphene loading. Under magnetic stirring the mixture was heated to 40°C and the solvent was allowed to evaporate until a thick black viscous liquid had formed. The beaker was then removed from the heat and left to stand for 12hrs to ensure that all the solvent had evaporated. The resulting composite was removed from the beaker and repeatedly folded over itself to ensure homogeneity of the sample.

Graphene-Sylgard

0.4g of Sylgard 170® (Dow Corning) Part A and Part B were added to a beaker containing 10ml of the graphene-IPA dispersion and stirred under magnetic stirring for 2 minutes. Further graphene-IPA was then added depending on the required graphene loading. The mixture was gently heated to 40°C and solvent was allowed to evaporate under continuous stirring. Once almost all solvent the solvent had evaporated the mixture was transferred into Teflon moulds (35×35mm). The mixture was left to stand for 12hrs to ensure complete solvent evaporation and then cured at 100°C for 1hr in an oven. The final composite was removed from the mould and measured ~600um in thickness. Details on composite characterisation can be found in the SI

Supporting Information. Detailed methods, derivations, detailed characterisation, literature data and fits, fit parameters.

ACKNOWLEDGEMENTS: We acknowledge the European Research Council Advanced Grant (FUTURE-PRINT), the European Union under Graphene Flagship cores 2 & 3 (grant agreements 785219 and 881603) and the Irish Research Council (GOIPG/2018/2000). We have also received support from the Science Foundation Ireland (SFI) funded centre AMBER (SFI/12/RC/2278) and availed of the facilities of the SFI-funded AML and ARM labs.

FIGURES

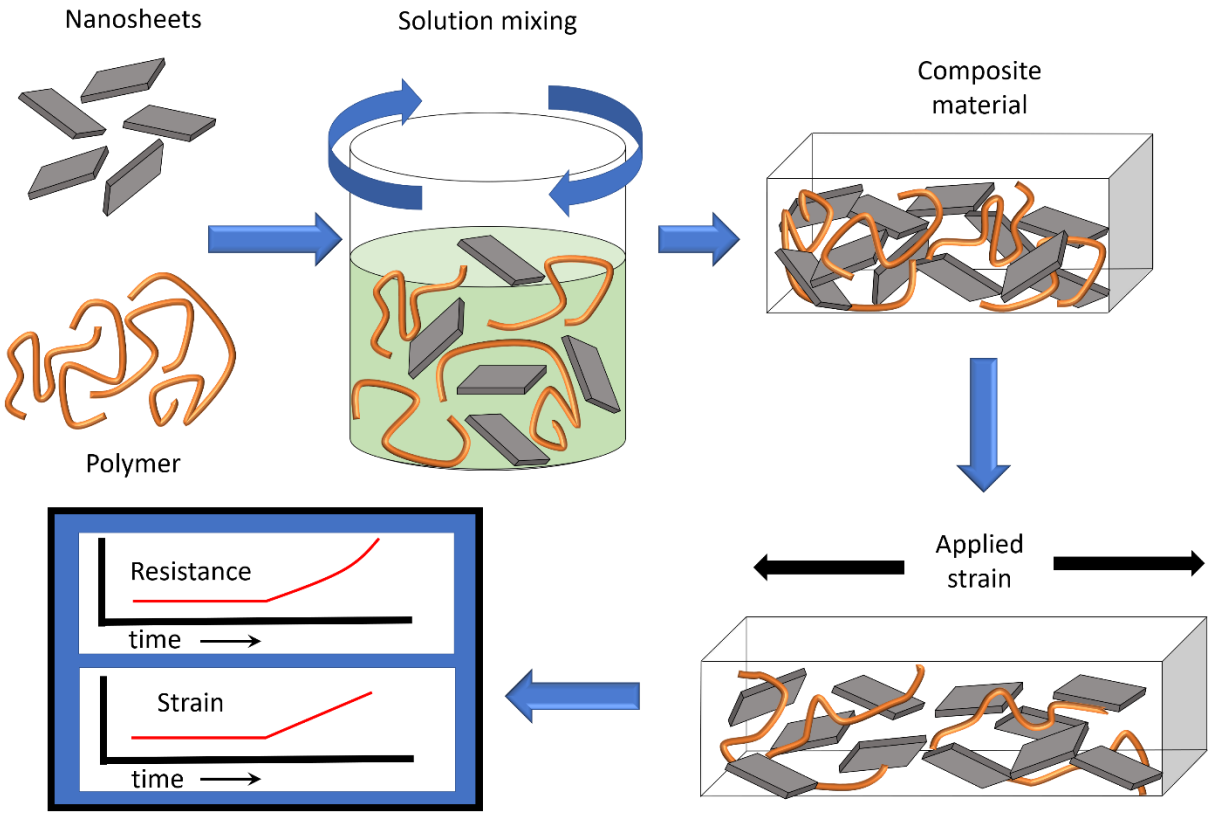

Schematic 1: Nanosheets and polymer are mixed in solution to yield composite suspensions. The solvent can be removed to yield a polymer-nanosheet composite. Applying strain to this composite deforms the nanosheet network, resulting in a change in its resistance.

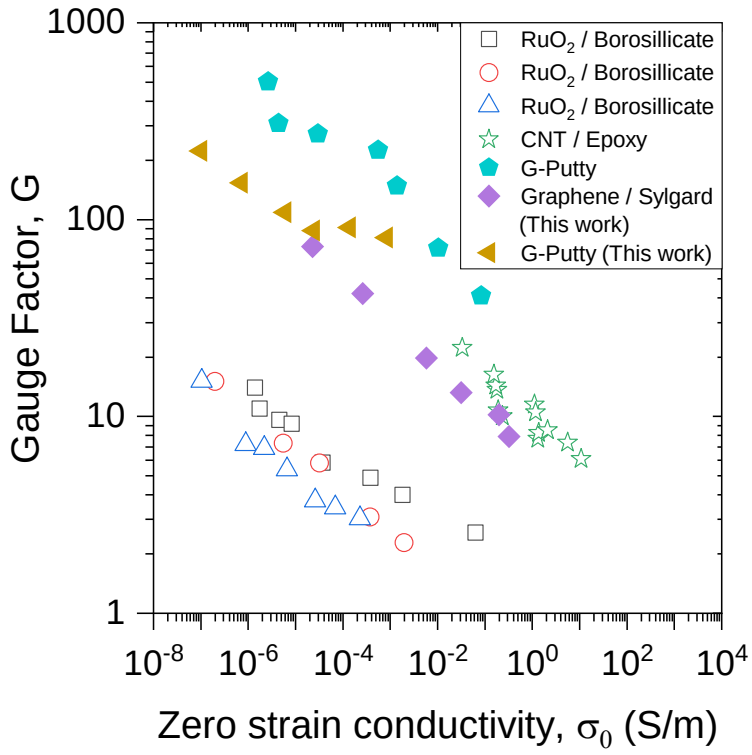

Figure 1: Literature data[15, 19, 48] as well as data collected here for Gauge factor (G) as a function of zero-strain conductivity (σ_0) for a range of nanocomposites (see SI for more data). All plots indicate an approximate power law relationship between these parameters.

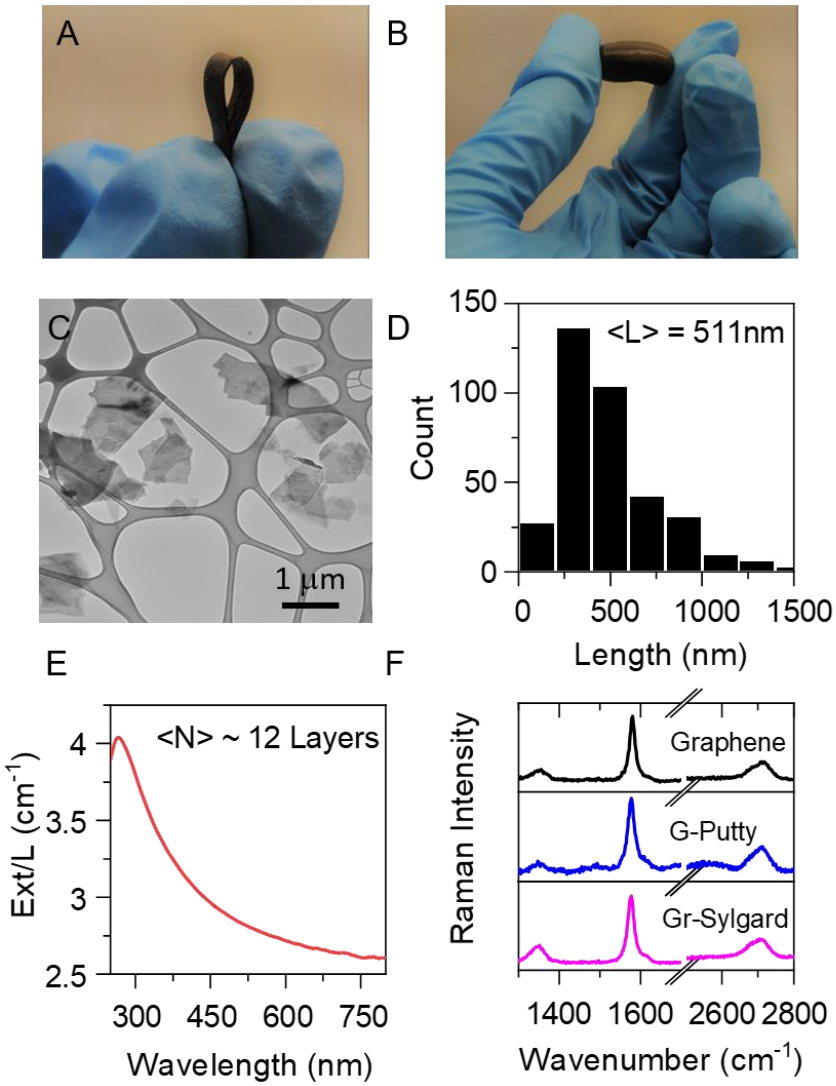

Figure 2: Characterisation of G-putty and graphene-sylgard composites: A-B) Photograph of graphene-sylgard (A) and G-putty (B) composites. C) TEM images of graphene flakes used in composite fabrication. D) Histogram of Nanosheet length <L> = 511m, was acquired through analysis of 368 nanosheets E) Uv-vis extinction spectra of graphene dispersion used to make composites with nanosheet thickness estimated using published metrics: <N> ~ 12 layers, F) Raman spectra for graphene nanosheets as well as G-putty and graphene-sylgard composites.

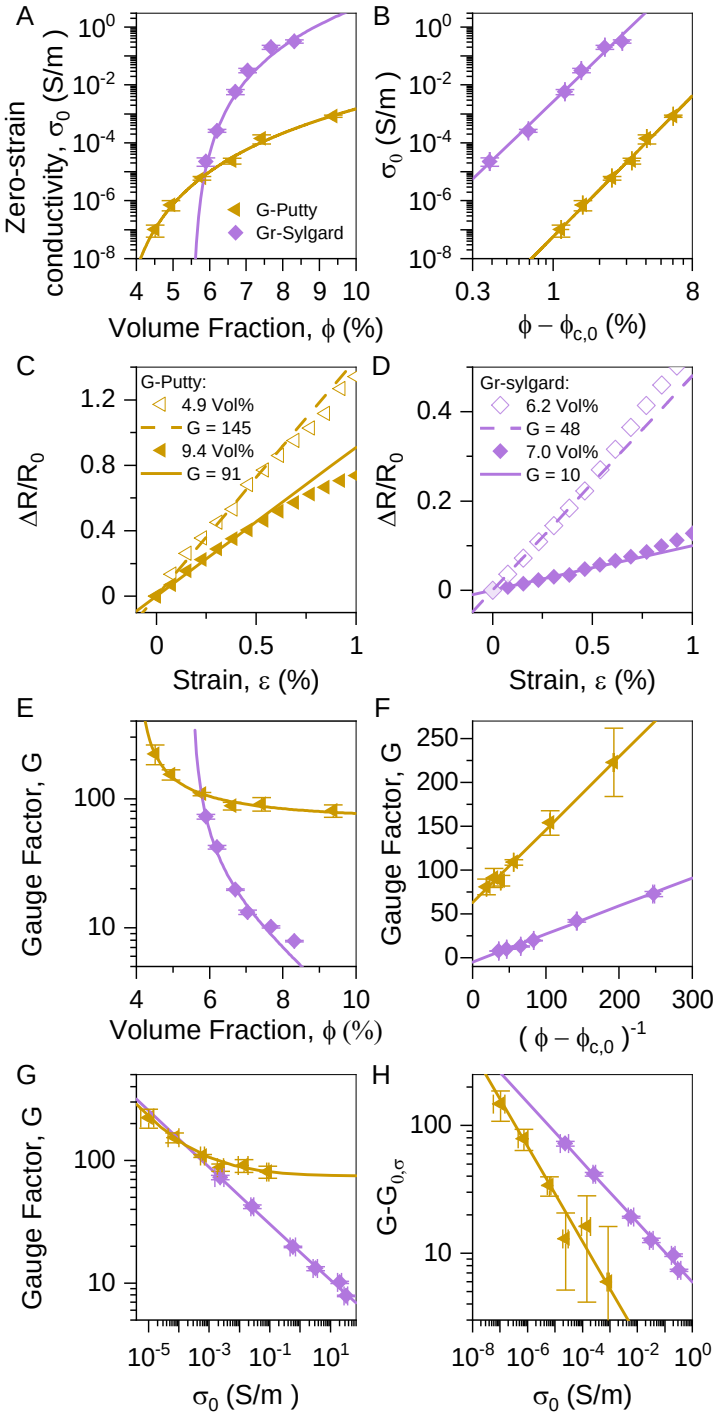

Figure 3: Electromechanical data for polymer-graphene composites prepared and tested during this work. The composites were prepared as described in the text using two different polysiloxane-based polymers filled with liquid-exfoliated graphene. A-B) Zero-strain conductivity plotted as a function of A) graphene volume fraction, ϕ, and B) zero-strain reduced volume fraction, ϕ-$\phi_{c,0}$. The solid lines are fits to the percolation scaling law, Eq.1 G-putty: ($\sigma_{c,0}$ = 3.3 × 10^3 S/m, $\phi_{c,0}$ = 3.39% and t_0 = 5.38), graphene-sylgard: ($\sigma_{c,0}$ = 4.60 ×

10^7 S/m, $\phi_{c,0}$ = 5.51% and t_0 = 5.12). C-D) Fractional resistance change plotted versus strain for two different graphene loading levels for the G-putty composites (C) and graphene-sylgard composites (D). E-F) Gauge factor plotted versus E) graphene volume fraction, ϕ, and F) inverse of zero-strain reduced volume fraction, $(\phi-\phi_{c,0})^{-1}$. The solid lines are fits to equation 5a. G-putty: ($\phi_{c,0}$ = 3.99% , G_1 = 0.83, $G_{0,\phi}$ = 63), graphene-syglard: ($\phi_{c,0}$ = 5.51%, G_1 = 0.32, $G_{0,\phi}$ = -5). G-H) Gauge factor versus conductivity data plotted as G vs. σ_0 (G) and G-$G_{0,\sigma}$ vs. σ_0 (H). The solid line is a fit to Eq.5b. G-putty: (t_0 = 2.7, s_1 = 0.41, $G_{0,\sigma}$ = 75), graphene-syglard: (t_0 = 4.3, s_1 = 6, $G_{0,\sigma}$ = 0.5).

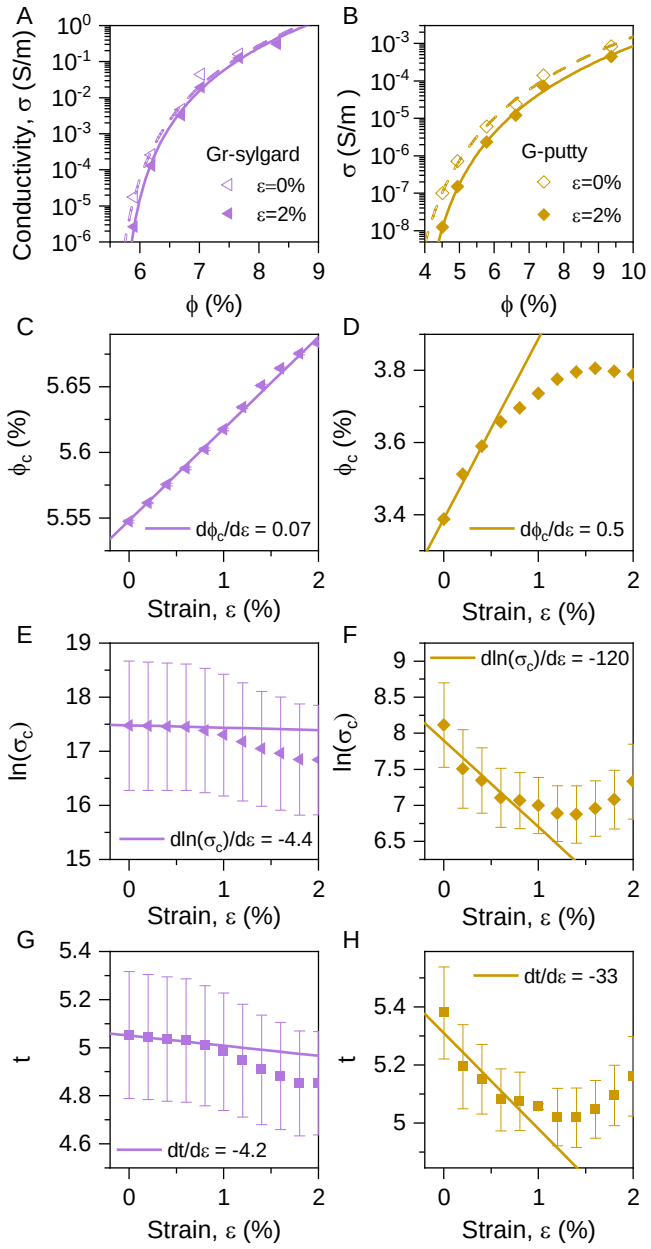

Figure 4: Strain dependent percolation data. A-B) Composite conductivity plotted versus graphene volume fraction for the G-putty composites (A) and graphene-sylgard composites (B). The lines are fits to the percolation scaling law (Eq.1) which outputs the fit parameters $\sigma_{c,0}$, $\phi_{c,0}$ and t_0. For both composites, such fits were obtained for a range of strain values. C-H) Plots of percolation parameters, ln(σ_c) (E-F), percolation exponent, *t*, (G-H) and percolation threshold, ϕ_c (C-D), all plotted versus strain for both composite types (graphene-sylgard in left column, G-putty in right column). The lines represent linear fits which give the slope of the curves at low strain.

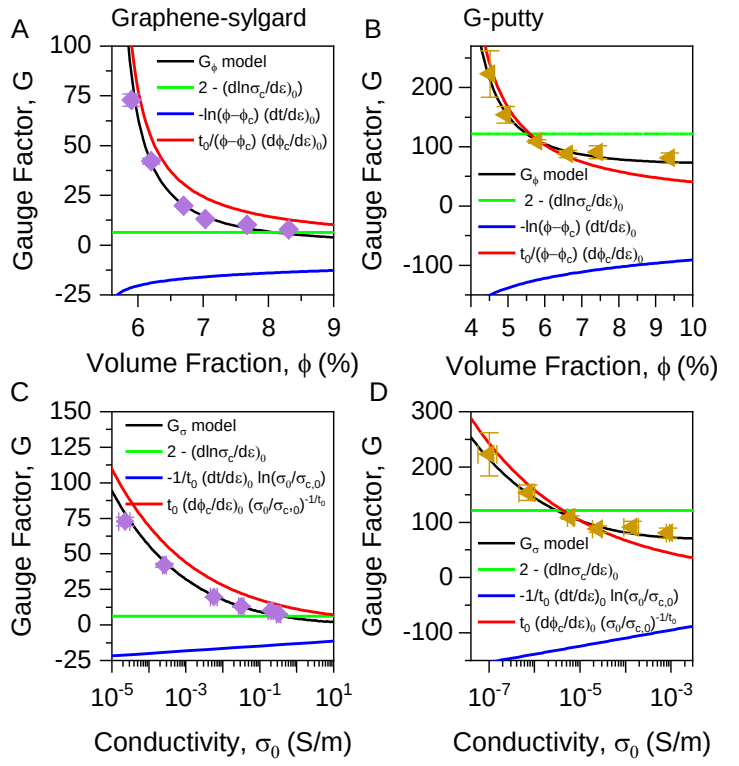

Figure 5: Plotting model predictions. Experimental gauge factor data plotted versus graphene volume fraction (A-B) and zero-strain conductivity (C-D) for graphene-sylgard (A,C) and G-putty (B,D) composites. In each panel, the black lines are obtained by plotting either equation 5b (A-B) or 5a (C-D) using the parameters obtained in figure 3. In each panel, the green, blue and red lines represent the first, second and third terms respectively in equations 5a and 5b.

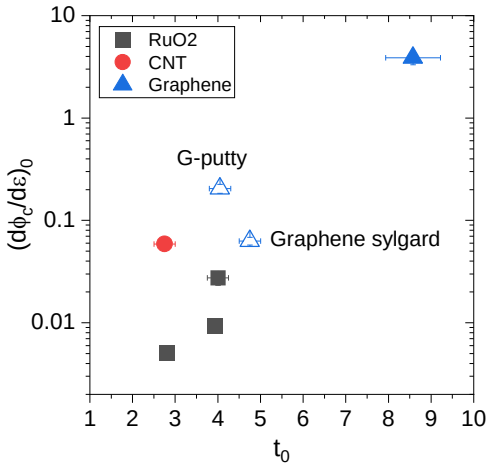

Figure 6: Values of $\left(d\phi_c / d\varepsilon\right)_0$ plotted versus t_0 for the literature data reported in figure 1 (solid symbols, see SI for fits) as well as the samples prepared in this work (open symbols). The values for t_0 are the averages of the values found by fitting the σ_0 vs. ϕ and G vs. σ_0 data sets.

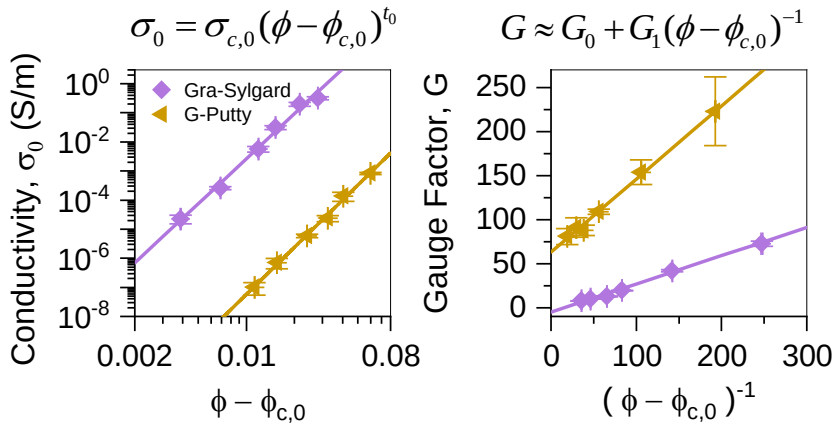

ToC fig

Table 1: Various parameters obtained from linearized fits of data to Equations 1 (σ_0 vs. ϕ), 5a (G vs. ϕ) and 5b (G vs. σ_0). Corresponding plots are shown in Figure 2 (B,F and H).

	G- sylgard	G-putty
From fitting σ_0 vs. ϕ		
$Ln(\sigma_{c,0})$	17.6 ± 1.1	8.1 ± 0.6
$\phi_{c,0}$	0.055 ± 0.01	0.034 ± 0.01
t_0	5.1 ± 0.2	5.4 ± 0.3
From fitting G vs. ϕ		
$G_{0,\phi}$	-5 ±	63 ±
G_1	0.32 ±	0.83 ±
$\phi_{c,0}$	0.055 ± 0.001	0.040 ± 0.001
From fitting G vs. σ_0		
$G_{0,\sigma}$	0.5 ± 0.1	75 ± 5
σ_1 (S/m)	2220 ± 110	0.084 ± 0.042

t_0	4.27 ± 0.20	2.7 ± 0.3

Table 2: Parameter values (Equation 4a,b,c) obtained from linear fits at low strain to the percolation data presented in Figure 3 (C-H).

	$\left(d\ln\sigma_c / d\varepsilon\right)_0$	$\left(d\phi_c / d\varepsilon\right)_0$	$\left(dt / d\varepsilon\right)_0$
Expected sign	-ve	+ve	-ve
G-Sylgard value	-4.4	0.07	-4.2
G-putty value	-120	0.5	-33

SUPPOSRTING INFORMATION

Composite characterisation methods; electromechanical composite characterisation; extracted fit parameters and fitted data from literature sources

References

1. Dong, Q.; Wang, X.; Liu, H.; Ryu, H.; Zhao, J.; Li, B.; Lei, Y., Heterogeneous Iridium Oxide/Gold Nanocluster for Non-enzymatic Glucose Sensing and pH Probing. *Engineered Science* **2019,** *8*, 46-53.
2. Xiang, X.; Pan, F.; Li, Y., Flower-like Bismuth Metal-Organic Frameworks Grown on Carbon Paper as a Free-Standing Electrode for Efficient Electrochemical Sensing of Cd2+ and Pb2+ in Water. *Engineered Science* **2018,** *3*, 77-83.
3. Fiorillo, A. S.; Critello, C. D.; Pullano, S. A., Theory, technology and applications of piezoresistive sensors: A review. *Sensor Actuat a-Phys* **2018,** *281*, 156-175.
4. Amjadi, M.; Kyung, K. U.; Park, I.; Sitti, M., Stretchable, Skin-Mountable, and Wearable Strain Sensors and Their Potential Applications: A Review. *Adv Funct Mater* **2016,** *26* (11), 1678-1698.
5. Boland, C. S., Stumbling through the Research Wilderness, Standard Methods To Shine Light on Electrically Conductive Nanocomposites for Future Healthcare Monitoring. *Acs Nano* **2019,** *13* (12), 13627-13636.
6. O'Driscoll, D. P.; McMahon, S.; Garcia, J.; Biccai, S.; Kelly, A. G.; Barwich, S.; Moebius, M.; Boland, C. S.; Coleman, J. N., Printable G-putty for Frequency and Rate Independent, High Performance Strain Sensors *Small* **2020,** *submitted*.
7. Window, A. L., *Strain gauge technology*. Springer: 1992; p 358.
8. Wu, Z.; Li, L.; Guo, N.; Yang, R.; Jiang, D.; Zhang, M.; Zhang, M.; Huang, Y.; Guo, Z., Effect of A Vinyl Ester-Carbon Nanotubes Sizing Agent on Interfacial Properties of Carbon

Fibers Reinforced Unsaturated Polyester Composites. *ES Materials & Manufacturing* **2019,** *6*, 38-48.
9. Chen, Y.; Wang, Y.; Su, T.; Chen, J.; Zhang, C.; Lai, X.; Jiang, D.; Wu, Z.; Sun, C.; Li, B.; Guo, Z., Self-Healing Polymer Composites Based on Hydrogen Bond Reinforced with Graphene Oxide. *ES Materials & Manufacturing* **2019,** *4*, 31-37.
10. Lyu, L.; Liu, J.; Liu, H.; Liu, C.; Lu, Y.; Sun, K.; Fan, R.; Wang, N.; Lu, N.; Guo, Z.; Wujcik, E. K., An Overview of Electrically Conductive Polymer Nanocomposites toward Electromagnetic Interference Shielding. *Engineered Science* **2018,** *2*, 26-42.
11. Yu, B.; Li, X.; An, J.; Jiang, Z.; Yang, J., Interfacial and Glass Transition Properties of Surface-Treated Carbon Fiber Reinforced Polymer Composites under Hygrothermal Conditions. *Engineered Science* **2018,** *2*, 67-73.
12. Zhao, H.; Chen, L.; Yun, J.; Tang, L.; Wen, Z.; Zhang, X.; Gu, J., Improved Thermal Stabilities, Ablation and Mechanical Properties for Carbon Fibers/Phenolic Resins Laminated Composites Modified by Silicon-containing Polyborazine. *Engineered Science* **2018,** *2*, 57–66.
13. Amjadi, M.; Kyung, K.-U.; Park, I.; Sitti, M., Stretchable, Skin-Mountable, and Wearable Strain Sensors and Their Potential Applications: A Review. *Adv Funct Mater* **2016,** *26* (11), 1678-1698.
14. Zhu, S.-E.; Krishna Ghatkesar, M.; Zhang, C.; Janssen, G. C. A. M., Graphene based piezoresistive pressure sensor. *Appl Phys Lett* **2013,** *102* (16), 161904.
15. Boland, C. S.; Khan, U.; Ryan, G.; Barwich, S.; Charifou, R.; Harvey, A.; Backes, C.; Li, Z.; Ferreira, M. S.; Möbius, M. E.; Young, R. J.; Coleman, J. N., Sensitive electromechanical sensors using viscoelastic graphene-polymer nanocomposites. *Science* **2016,** *354* (6317), 1257-1260.
16. Boland, C. S.; Khan, U.; Backes, C.; O'Neill, A.; McCauley, J.; Duane, S.; Shanker, R.; Liu, Y.; Jurewicz, I.; Dalton, A. B.; Coleman, J. N., Sensitive, high-strain, high-rate bodily motion sensors based on graphene-rubber composites. *Acs Nano* **2014,** *8* (9), 8819-8830.
17. Marsden, A. J.; Papageorgiou, D. G.; Vallés, C.; Liscio, A.; Palermo, V.; Bissett, M. A.; Young, R. J.; Kinloch, I. A., Electrical percolation in graphene–polymer composites. *2d Mater* **2018,** *5* (3), 032003.
18. Lynch, P. J.; Ogilvie, S. P.; Large, M. J.; Graf, A. A.; O'Mara, M. A.; Taylor, J.; Salvage, J. P.; Dalton, A. B., Graphene-based printable conductors for cyclable strain sensors on elastomeric substrates. *Carbon* **2020,** *169*, 25-31.
19. Hu, N.; Karube, Y.; Arai, M.; Watanabe, T.; Yan, C.; Li, Y.; Liu, Y. L.; Fukunaga, H., Investigation on sensitivity of a polymer/carbon nanotube composite strain sensor. *Carbon* **2010,** *48* (3), 680-687.
20. Alamusi; Hu, N.; Fukunaga, H.; Atobe, S.; Liu, Y. L.; Li, J. H., Piezoresistive Strain Sensors Made from Carbon Nanotubes Based Polymer Nanocomposites. *Sensors-Basel* **2011,** *11* (11), 10691-10723.
21. Wang, S.; Zhang, X.; Wu, X.; Lu, C., Tailoring percolating conductive networks of natural rubber composites for flexible strain sensors via a cellulose nanocrystal templated assembly. *Soft Matter* **2016,** *12* (3), 845-852.
22. Levin, Z. S.; Robert, C.; Feller, J. F.; Castro, M.; Grunlan, J. C., Flexible latex—polyaniline segregated network composite coating capable of measuring large strain on epoxy. *Smart Materials and Structures* **2013,** *22* (1), 015008.
23. Shintake, J.; Piskarev, E.; Jeong, S. H.; Floreano, D., Ultrastretchable Strain Sensors Using Carbon Black-Filled Elastomer Composites and Comparison of Capacitive Versus Resistive Sensors. *Adv Mater Technol-Us* **2018,** *3* (3), 1700284.
24. Narongthong, J.; Le, H. H.; Das, A.; Sirisinha, C.; Wießner, S., Ionic liquid enabled electrical-strain tuning capability of carbon black based conductive polymer composites for

small-strain sensors and stretchable conductors. *Composites Science and Technology* **2019,** *174*, 202-211.
25. Amjadi, M.; Pichitpajongkit, A.; Lee, S.; Ryu, S.; Park, I., Highly stretchable and sensitive strain sensor based on silver nanowire-elastomer nanocomposite. *Acs Nano* **2014,** *8* (5), 5154-5163.
26. Zhu, J.; Wei, S.; Ryu, J.; Guo, Z., Strain-sensing elastomer/carbon nanofiber "metacomposites". *Journal of Physical Chemistry C* **2011,** *115* (27), 13215-13222.
27. Kim, H. J.; Thukral, A.; Yu, C., Highly sensitive and very stretchable strain sensor based on a rubbery semiconductor. *ACS Applied Materials and Interfaces* **2018,** *10* (5), 5000-5006.
28. Biccai, S.; Boland, C. S.; O'Driscoll, D. P.; Harvey, A.; Gabbett, C.; O'Suilleabhain, D. R.; Griffin, A. J.; Li, Z.; Young, R. J.; Coleman, J. N., Negative Gauge Factor Piezoresistive Composites Based on Polymers Filled with MoS2 Nanosheets. *Acs Nano* **2019,** *13* (6), 6845-6855.
29. Bauhofer, W.; Kovacs, J. Z., A review and analysis of electrical percolation in carbon nanotube polymer composites. *Composites Science and Technology* **2009,** *69* (10), 1486-1498.
30. Rahman, R.; Servati, P., Effects of inter-tube distance and alignment on tunnelling resistance and strain sensitivity of nanotube/polymer composite films. *Nanotechnology* **2012,** *23* (5), 055703.
31. Yang, H.; Yuan, L.; Yao, X.; Fang, D., Piezoresistive response of graphene rubber composites considering the tunneling effect. *Journal of the Mechanics and Physics of Solids* **2020,** *139*, 103943.
32. Zhang, R.; Baxendale, M.; Peijs, T., Universal resistivity-strain dependence of carbon nanotube/polymer composites. *Physical Review B - Condensed Matter and Materials Physics* **2007,** *76* (19), 195433.
33. Liu, J.; Zhao, F.; Tao, Q.; Cao, J.; Yu, Y.; Zhang, X., Visualized simulation for the nanostructure design of flexible strain sensors: from a numerical model to experimental verification. *Materials Horizons* **2019,** *6* (9), 1892-1898.
34. Cao, J.; Zhang, X., Modulating the percolation network of polymer nanocomposites for flexible sensors. *Journal of Applied Physics* **2020,** *128* (22), 220901.
35. Wescott, J. T.; Kung, P.; Maiti, A., Conductivity of carbon nanotube polymer composites. *Appl Phys Lett* **2007,** *90* (3), 033116.
36. Kuilla, T.; Bhadra, S.; Yao, D. H.; Kim, N. H.; Bose, S.; Lee, J. H., Recent advances in graphene based polymer composites. *Prog Polym Sci* **2010,** *35* (11), 1350-1375.
37. Johner, N.; Grimaldi, C.; Balberg, I.; Ryser, P., Transport exponent in a three-dimensional continuum tunneling-percolation model. *Phys Rev B* **2008,** *77* (17), 174204.
38. Foygel, M.; Morris, R. D.; Anez, D.; French, S.; Sobolev, V. L., Theoretical and computational studies of carbon nanotube composites and suspensions: Electrical and thermal conductivity. *Phys Rev B* **2005,** *71* (10), 104201.
39. Garboczi, E. J.; Snyder, K. A.; Douglas, J. F.; Thorpe, M. F., Geometrical percolation threshold of overlapping ellipsoids. *Physical Review E* **1995,** *52* (1), 819-828.
40. Pu, J. H.; Zha, X. J.; Zhao, M.; Li, S.; Bao, R. Y.; Liu, Z. Y.; Xie, B. H.; Yang, M. B.; Guo, Z.; Yang, W., 2D end-to-end carbon nanotube conductive networks in polymer nanocomposites: A conceptual design to dramatically enhance the sensitivities of strain sensors. *Nanoscale* **2018,** *10* (5), 2191-2198.
41. Du, F.; Fischer, J. E.; Winey, K. I., Effect of nanotube alignment on percolation conductivity in carbon nanotube/polymer composites. *Physical Review B - Condensed Matter and Materials Physics* **2005,** *72* (12), 121404.

42. Cunningham, G.; Lotya, M.; McEvoy, N.; Duesberg, G. S.; van der Schoot, P.; Coleman, J. N., Percolation scaling in composites of exfoliated MoS2 filled with nanotubes and graphene. *Nanoscale* **2012,** *4* (20), 6260-6264.
43. Guyot-Sionnest, P., Electrical Transport in Colloidal Quantum Dot Films. *Journal of Physical Chemistry Letters* **2012,** *3* (9), 1169-1175.
44. Balberg, I.; Azulay, D.; Goldstein, Y.; Jedrzejewski, J., Possible origin of the smaller-than-universal percolation-conductivity exponent in the continuum. *Phys Rev E* **2016,** *93* (6), 062132.
45. Balberg, I.; Azulay, D.; Toker, D.; Millo, O., Percolation and tunneling in composite materials. *Int J Mod Phys B* **2004,** *18* (15), 2091-2121.
46. Vionnet-Menot, S.; Grimaldi, C.; Maeder, T.; Strassler, S.; Ryser, P., Tunneling-percolation origin of nonuniversality: Theory and experiments. *Phys Rev B* **2005,** *71* (6), 064201.
47. Liu, H.; Li, Y.; Dai, K.; Zheng, G.; Liu, C.; Shen, C.; Yan, X.; Guo, J.; Guo, Z., Electrically conductive thermoplastic elastomer nanocomposites at ultralow graphene loading levels for strain sensor applications. *Journal of Materials Chemistry C* **2015,** *4* (1), 157-166.
48. Carcia, P. F.; Suna, A.; Childers, W. D., Electrical-Conduction and Strain Sensitivity in Ruo2 Thick-Film Resistors. *Journal of Applied Physics* **1983,** *54* (10), 6002-6008.
49. Christ, J. F.; Aliheidari, N.; Ameli, A.; Pötschke, P., 3D printed highly elastic strain sensors of multiwalled carbon nanotube/thermoplastic polyurethane nanocomposites. *Materials and Design* **2017,** *131*, 394-401.
50. Gao, J.; Wang, X.; Zhai, W.; Liu, H.; Zheng, G.; Dai, K.; Mi, L.; Liu, C.; Shen, C., Ultrastretchable Multilayered Fiber with a Hollow-Monolith Structure for High-Performance Strain Sensor. *ACS Applied Materials and Interfaces* **2018,** *10* (40), 34592-34603.
51. Kang, I.; Schulz, M. J.; Kim, J. H.; Shanov, V.; Shi, D., A carbon nanotube strain sensor for structural health monitoring. *Smart Materials and Structures* **2006,** *15* (3), 737.
52. Kim, J. H.; Hwang, J. Y.; Hwang, H. R.; Kim, H. S.; Lee, J. H.; Seo, J. W.; Shin, U. S.; Lee, S. H., Simple and cost-effective method of highly conductive and elastic carbon nanotube/polydimethylsiloxane composite for wearable electronics. *Scientific Reports* **2018,** *8* (1), 1-11.
53. Wang, B.; Lee, B. K.; Kwak, M. J.; Lee, D. W., Graphene/polydimethylsiloxane nanocomposite strain sensor. *Review of Scientific Instruments* **2013,** *84* (10), 105005.
54. Stankovich, S.; Dikin, D. A.; Dommett, G. H. B.; Kohlhaas, K. M.; Zimney, E. J.; Stach, E. A.; Piner, R. D.; Nguyen, S. T.; Ruoff, R. S., Graphene-based composite materials. *Nature* **2006,** *442* (7100), 282-286.
55. Grillard, F.; Jaillet, C.; Zakri, C.; Miaudet, P.; Derre, A.; Korzhenko, A.; Gaillard, P.; Poulin, P., Conductivity and percolation of nanotube based polymer composites in extensional deformations. *Polymer* **2012,** *53* (1), 183-187.
56. O'Driscoll, D. P.; Vega-Mayoral, V.; Harley, I.; Boland, C. S.; Coleman, J. N., Optimising composite viscosity leads to high sensitivity electromechancial sensors. *2D Materials* **2018,** *5* (3), 035042.
57. Backes, C.; Paton, K. R.; Hanlon, D.; Yuan, S.; Katsnelson, M. I.; Houston, J.; Smith, R. J.; McCloskey, D.; Donegan, J. F.; Coleman, J. N., Spectroscopic metrics allow in situ measurement of mean size and thickness of liquid-exfoliated few-layer graphene nanosheets. *Nanoscale* **2016,** *8* (7), 4311-23.
58. Wu, S.; Ladani, R. B.; Zhang, J.; Bafekrpour, E.; Ghorbani, K.; Mouritz, A. P.; Kinloch, A. J.; Wang, C. H., Aligning multilayer graphene flakes with an external electric field to improve multifunctional properties of epoxy nanocomposites. *Carbon* **2015,** *94*, 607-618.

59. White, S. I.; DiDonna, B. A.; Mu, M. F.; Lubensky, T. C.; Winey, K. I., Simulations and electrical conductivity of percolated networks of finite rods with various degrees of axial alignment. *Phys Rev B* **2009,** *79* (2), 024301.